Maximum Entropy and the Nearly Black Object

By

David L. Donoho* Iain M. Johnstone† Jeffrey C. Hoch+
Alan S. Stern#

Technical Report No. 213
August 1989

*University of California, Berkeley. Supported by NSF DMS 84-51753, and by grants from Schlumberger-Doll, and Western Geophysical.

†Stanford University. Supported by NSF DMS 84-51750, by SERC, and by the Sloan Foundation.

+#Rowland Institute for Science, Cambridge, Mass.

Department of Statistics
University of California
Berkeley, California

Maximum Entropy and the Nearly Black Object

David L. Donoho* Iain M. Johnstone† Jeffrey C. Hoch‡
Alan S. Stern‡

March, 1990

Abstract

Maximum Entropy Inversion (ME) is a nonlinear inversion technique for inverse problems where the object to be recovered is known to be positive. It has been applied in areas ranging from Radio Astronomy to various forms of Spectroscopy, sometimes with dramatic success. In some cases, ME has attained an order of magnitude finer resolution and/or an order of magnitude smaller noise level than that obtainable by standard linear methods.

The dramatic sucesses all seem to occur in cases where the object to be recovered is 'nearly black': essentially zero in the vast majority of samples. We show that near-blackness is *required*, both for signal-to-noise enhancements, and for superresolution. However, other methods – in particular, minimum l_1-norm reconstruction – may exploit near-blackness to an even greater extent.

Key Words and Phrases. Inverse Problems. Positivity Constraints. Magnetic Resonance Spectroscopy. Diffraction-limited imaging. Super-Resolution. Nonlinear recovery. Minimax Decision Theory.

*University of California, Berkeley. Supported by NSF DMS 84-51753, and by grants from Apple Computer, Schlumberger-Doll Research, and Western Geophysical.

†Stanford University. Supported by NSF DMS 84-51750, by SERC, and by the Sloan Foundation.

‡♯Rowland Institute for Science, Cambridge Mass.

1 Introduction

Maximum Entropy Inversion is a technique for solving ill-posed inverse problems arising in science and engineering. These problems may be formalized as follows. A very high-dimensional vector x describes an unknown object (for example signal amplitudes at various times, or intensities of light in various pixels of an image). We are unable to measure x directly, however. Instead, we get a vector y of *noisy*, *indirect* observations:

$$y = Kx + z \tag{1}$$

where K is a *known* linear operator, and z represents noise. It is possible to model problems in tomography, spectroscopy, astronomy, and other fields in this way, by specifying K appropriately, as a discrete form of some mathematical transform, such as a Radon, Fourier, or convolution transform [3,19,1]. (Still other problems, such as crystallography, might be handled as well, if K were allowed to be a nonlinear transformation [21,2], but we do not consider that possibility in this paper.)

The key element in many of these problems is that they are *ill-posed*. While this may be expressed in various ways at a physical level, at a mathematical level, ill-posedness occurs when the effective dimension of y is considerably smaller than the dimension of x; i.e. when the operator K has few singular values which are significantly different from zero [3,19,1]. In one of the most common examples, image deblurring, K would be a smoothing transform, with singular values small at singular vectors corresponding to high frequencies, so that the detailed high-frequency information in x is lost; the inverse problem is to recover x, with high frequencies restored (if possible).

Were it not for the ill-posedness, it would be natural to approach the problem by least squares. After all (1) is just a linear model, and an estimate of x can be obtained from the least-squares principle $\hat{x}_{LS} = \arg\min_x ||y - Kx||_2^2$, giving $\hat{x}_{LS} = (K^T K)^{-1} K^T y$. However, because of ill-posedness, this estimate is either undefined, or else has very poor performance, even if one

interprets the matrix inverse as a generalized inverse. It is by now traditional to approach such problems by least-squares regularization. Then one estimates x by the solution to the optimization problem $\hat{x} = \arg\min_x ||y - Kx||_2^2 + \lambda||x||_2^2$, which gives the formula $\hat{x}_{RLS} = (K^T K + \lambda I)^{-1} K^T y$. Here λ is a tuning constant specified by the user in some way. Of course this idea has been used in many, many fields and also goes by many other names, such as ridge regression, penalized likelihood, Bayesian posterior mean, and damped least squares.

In this paper we focus on problems where the object x to be recovered has nonnegative coordinates. Think of images, chemical spectra, or other measurements of intensities. In this context, Maximum Entropy Inversion (ME) [13] is a regularization method which gives an estimate of x by the prescription

$$\max_x \; -\sum_i x_i \log x_i \text{ subject to } ||y - Kx||_2^2 \leq S^2; \qquad (2)$$

see also [27,11] for related definitions of ME. We prefer to define it in the equivalent form

$$\hat{x}_{ME} = \arg\min_x ||y - Kx||_2^2 + 2\lambda \sum_i x_i \log x_i, \qquad (3)$$

which emphasizes the similarity to regularized least squares. This way of stating the problem is equivalent, in that there is a (data-dependent) one-one correspondence between λ in (3) and S in (2) which makes the two optimization problems have the same solution.

Although ME has a formal similarity with least-squares regularization – one is, after all just replacing the quadratic penalty $\sum x_i^2$ with $\sum x_i \log x_i$ – there are important differences. Because of properties of the entropy $H(x) = -\sum x_i \log x_i$, the solution to (3) must always have nonnegative entries. Second, because the objective in (3) is not quadratic, the solution is not linear in the observations vector y. Finally, no closed form expression is known for the solution of (3). Instead, (3) must be approached as a general convex optimization problem, and solved by some

variant of gradient descent. However, special purpose optimizers for this problem have been developed [24] which can solve very high dimensional problems.

The implicit claim made by advocates and users of maximum entropy inversion is that these differences from least-squares regularization matter: that the positivity and nonlinearity of the ME process provide benefits in applications which are worth the computational expense of ME.

In fact, many applications of ME have been developed: to problems in NMR spectroscopy [22]; in astronomy (interferometry) [13]; and in infrared absorption spectroscopy [11]. Many published reconstructions obtained via ME are excellent, and a few side-by-side comparisons show that ME regularization can, in certain cases, dramatically outperform quadratic regularization.

We mention two protypical examples. (A) Sibisi et al. [22] compare the ME reconstruction of an NMR spectrum with reconstruction by conventional (least-squares) methods (Figure 1.1). Not only does the ME reconstruction look nicer (notice the lack of noisy oscillations), but ME does a better job, in an objective sense. The ME reconstruction resembles closely the reconstruction which conventional methods could obtain only on data from a much more sensitive experiment i.e. an experiment with higher signal-to-noise ratio.

(B) B.R. Frieden [11] shows that ME can sometimes *superresolve*. We shall explain terminology in section 4; but we illustrate the point with Frieden's diagram. Figure 1.2 shows a true, 'spiky' object, a least-squares reconstruction, and an ME reconstruction. In this case, the true object consists of two closely spaced spikes; and the data are diffraction-limited. The reconstruction by ME clearly shows the presence of two spikes, the reconstruction by least-squares does not. The term 'superresolution' is used here because ME in this case resolves better than the so-called *Rayleigh limit*, a resolution limit which all linear translation-invariant least squares methods must obey. In particular, the two spikes are spaced less than 1/3 of the Rayleigh distance apart, yet the ME reconstruction resolves them.

These examples illustrate the basic phenomena that sometimes occur with ME reconstructions:

- (A) *signal-to-noise* enhancement; and
- (B) *superresolution.*

The purpose of our paper is to explain how and why these phenomena occur, and particularly *when* (i.e. under what conditions) they occur. We hope to make three main points.

[I] The phenomena are real, and due to the nonlinearity of ME. However, they are delicate, and they occur if and only if the image to be recovered is *nearly black* – nearly zero in all but a small fraction of samples.

[II] ME is not the only nonlinear inversion technique able to exploit near-blackness and produce these phenomena. For example, another method, l_1-reconstruction, can do so optimally, from one point of view.

[III] The improvements obtained by such nonlinear processing do not fully substitute for improving the sensitivity by getting a better experiment.

The paper is organized as follows. Section 2 discusses a simple estimation problem in which it can be shown how the nonlinear behavior of ME allows for an improvement in signal-to-noise ratio (Phenomenon (A)). Section 3 shows how this surprisingly simple analysis extends to studying the behavior of ME inversion in NMR spectroscopy. Finally, Section 4 sketches a theory explaining superresolution, Phenomenon (B). For Summary and Discussion see Section 5. Section 6 contains proofs of Theorems.

Acknowledgements. The authors would like to thank M. Burns, B.R. Frieden, E. Gassiat, F.J. Gilbert, R.L. Parker, P.B. Stark, J.W. Tukey, and G. Wahba for interesting discussions and correspondence. B.F. Logan kindly provided a bound copy of his Ph. D. thesis. Lorenzo Sadun, Moxiu Mo, and Cha-Yong Koo (in chronological order) provided computing assistance.

2 Improving Signal-to-Noise Ratio

Consider the simple problem of estimating $x = (x_i)_{i=1}^n$ from noisy data y:

$$y_i = x_i + z_i, \quad i = 1, \ldots, n \tag{4}$$

where the noise terms z_i are independent and Normally distributed with variance σ^2. This is a special case of (1), with K the identity operator.

In this model, the ME estimate of (3) is the solution to

$$\hat{x} = \arg \min_{x=(x_i)} \sum_i (x_i - y_i)^2 + 2\lambda \sum_i x_i \log x_i \tag{5}$$

where only positive x's need be considered in the minimum. Taking partial derivatives, one finds that at the solution $(\hat{x}_i)$, say,

$$0 = 2\lambda(1 + \log \hat{x}_i) + 2(\hat{x}_i - y_i)$$

so that $\hat{x}_i$ is implicitly given as the solution to

$$y_i = \hat{x}_i + \lambda(1 + \log \hat{x}_i).$$

Let $\delta_{ME,\lambda}(y)$ be the solution to the equation

$$y = \delta + \lambda(1 + \log \delta).$$

Then the solution to (5) can be written explicitly in the form:

$$\hat{x}_i = \delta_{ME,\lambda}(y_i) \quad i = 1, \ldots, n. \tag{6}$$

In words, the ME estimate is the result of applying the simple nonlinearity $\delta_{ME,\lambda}$ coordinatewise.

Figure 2.1 displays the function $\delta_{ME,\lambda}(\cdot)$ for three different parameter values $\lambda = \frac{1}{10}, \frac{1}{2}, 2$. The nonlinearity is defined for both positive and negative arguments, is always positive, tends to zero for extreme negative arguments, and tends to ∞ for extreme positive arguments. The ME nonlinearity has a fixed point, $\delta_{ME,\lambda}(e^{-1}) = e^{-1}$, towards which the data are always "shrunk":

$$|\delta_{ME,\lambda}(y) - e^{-1}| < |y - e^{-1}|.$$

The amount of shrinkage, as measured by the left hand side, increases as λ increases. [1]

The effects this nonlinearity can produce are shown in figure 2.2. The top panel in this figure shows a "signal" x consisting mostly of zeros, and a few large spikes. The middle panel shows data y observed when the normal errors z have standard deviation 1. The bottom panel shows the ME estimate $\hat{x}$ obtained using $\lambda = \frac{1}{2}$. The ME estimate has many visual similarities to the "truth" in the top panel. There are only a few peaks standing out from a nearly constant background. To some readers, the transition from Panel (b) to Panel (c) will seem a dramatic visual improvement.

There is certainly a quantitative improvement. Define the mean squared error $\mathrm{MSE}(\hat{x}, x) = n^{-1} \sum_i (\hat{x}_i - x_i)^2$. Then the raw data of Panel b have $\mathrm{MSE}(y, x) \approx 1$, while for the estimate of Panel c we have $\mathrm{MSE}(\hat{x}, x) \approx .45$, a factor of 2 improvement.

2.1 Improvement and Near-Black Images

This improvement is due to the special nature of x used in Figure 2.2. Let Y be distributed $N(\theta, \sigma^2)$, and introduce the *risk* $\rho(\theta; \lambda, \sigma) = \mathrm{E}\ (\delta_{ME,\lambda}(Y) - \theta)^2$, the expectation referring to the distribution of Y. Then we have

$$\mathrm{E\ MSE}(\hat{x}, x) = \frac{1}{n} \sum_{i=1}^{n} \rho(x_i)$$

with expectation referring to model (4).

Figure 2.3 plots $\rho(\theta)$; the parameters λ and σ^2 were chosen exactly as in figure 2.2. Evidently, the risk ρ is small if and only if θ is near zero. Hence the expected MSE of $\hat{x}$ is small compared with σ^2 if and only if most coordinates of x are nearly zero. Indeed, one can read off the graph that

$$\mathrm{E\ MSE}(\hat{x}, x) \leq \epsilon\sigma^2$$

[1] The fixed point e^{-1}, or "default value", has an arbitrary character, and in the practice of ME, the objective is often modified by replacing $\log x_i$ by $\log(\beta x_i)$, where $exp(-\beta)/\beta = A$, which moves the fixed point from e^{-1} to A. Compare Section 3 below.

implies (by Markov's inequality)

$$\frac{1}{n}\#\{i : x_i \geq 2\sigma\} \leq \frac{5}{4}\epsilon$$

etc. The trivial estimate y has expected mean squared error σ^2. This shows that if ME improves significantly on the trivial estimate, then the true image must be significantly nonzero in only a small fraction of samples. Hence Figure 2.2 is in some sense the generic example of ME's ability to improve MSE in model (4).

2.2 Optimal Performance with Nearly Black Images

ME is not the only estimate that can be used in the model (4). Consider the optimization problem

$$\hat{x} = \arg \min_{x=(x_i)} \sum_i (x_i - y_i)^2 + 2\lambda \sum_i x_i \tag{7}$$

where now the minimum is over nonnegative x. We call this the minimum l_1-rule because it uses a penalty which is the same as the l_1-norm for nonnegative x. Repeating the analysis above, we see that the minimum l_1 estimate is obtained by applying a coordinatewise nonlinearity:

$$\hat{x}_i = \delta_{l_1,\lambda}(y_i), \quad i = 1, \ldots, n,$$

where $\delta_{l_1,\lambda}(y) \equiv \max(0, y - \lambda)$. Here one gets $\hat{x}_i$ by "pulling down" every measured observation y_i by an amount λ, taking care to ensure a nonnegative result.

If we were to display the analog of Figure 2.2c for this estimator we would, of course, get a plot visually resembling the 'true' answer for that situation, Figure 2.2a. The reader is invited to imagine this for himself.

It turns out that for "nearly black" images of the type in Figure 2.2a, the l_1 method does an excellent job quantitatively, and not just visually. Thus for the data of Figure 2.2b, the choice

$\lambda = \frac{1}{2}$ gives $\mathrm{MSE}(\delta_{l_1,\lambda}, x) \approx .3$. This is 50% better than ME and more than 3 times as good as the trivial estimate y.

In fact, the l_1 procedure has a certain optimality in dealing with nearly black images. We formalize this property by using minimax decision theory.

Definition 1 *The class $X_n(\epsilon)$ of ϵ-black images consists of all sequences of length n satisfying (1) $x_i \geq 0$ for all i, and (2) $\#\{i : x_i > 0\} \leq n\epsilon$.*

Suppose we have a rule $\hat{x} = \delta_n(y)$ for estimating x in a problem of size n. If this rule makes excellent use of the nearly-black property, then it should have a small expected MSE for any $x \in X_n(\epsilon)$. Thus, the following worst-case mean-squared error should be small:

$$M_n(\delta_n, \epsilon) = \sup_{x \in X_n(\epsilon)} E\,\mathrm{MSE}(\delta_n(y), x)$$

The smallest this can possibly be for any rule is

$$M_n(\epsilon) = \inf_{\delta_n} M_n(\delta_n, \epsilon).$$

A rule attaining this minimum is called *minimax*.

The class $X_n(\epsilon)$ contains all images which are nearly black: images in which the nonzero pixels can have any conceivable arrangement in space and in amplitude; $M_n(\epsilon)$ therefore measures how accurately it is possible to reconstruct x from y just using the information that $x \geq 0$ and that $x_i > 0$ in a small fraction of samples. The following result describes the behavior of

$$M(\epsilon) \equiv \sup_n M_n(\epsilon)$$

and shows that the l_1 rule is nearly minimax for small ϵ.

Theorem 1 *Let $\mathcal{F}_\epsilon$ be the class of distributions of nonnegative random variables which place at least $1 - \epsilon$ of their mass at 0. Then*

$$M(\epsilon) = \sigma^2 \sup\{1 - I(\Phi * F) : F \in \mathcal{F}_\epsilon\} \tag{8}$$

where $I(G) = \int (g')^2/g$ *is the Fisher Information. We have the asymptotic result*

$$M(\epsilon) = \sigma^2 \, 2\,\epsilon \log(\frac{1}{\epsilon}) \, (1 + o(1)) \;\; as \;\; \epsilon \to 0 \tag{9}$$

Moreover, let $M(l_1, \epsilon) = \inf_\lambda \sup_n M_n(\delta_{l_1,\lambda}, \epsilon)$ *denote the minimax performance among* l_1 *rules over all* ϵ*-black images. Then the optimal* λ *satisfies* $\lambda^2(\epsilon) \sim 2\log(\frac{1}{\epsilon})$ *and*

$$\frac{M(l_1, \epsilon)}{M(\epsilon)} \to 1 \quad as \; \epsilon \to 0. \tag{10}$$

The proof is in Section 6. Our analysis has several points of contact with work of Peter Bickel [5] and M.S. Pinsker [20].

We interpret (9) as follows. If we knew a priori which x_i were nonzero in x, we could always estimate the other x_i as zero and estimate the nonzero x_i by y_i. This would give $E\text{MSE} = \sigma^2\epsilon$. Relation (9) says that even without knowing a priori which x_i are nonzero, we can get an MSE which is worse only by logarithmic terms.

Table 1 illustrates the fact that (10) is a good approximation for ϵ as large as 5% or even 10%. Included for illustration is the behavior of a Bayes rule which assumes that the x_i are random variables, independent, and exponentially distributed; this rule does far worse than the l_1 rule.

Incidentally, ME is not competitive with l_1 in this worst-case analysis. As figure 2.2 shows, the risk of ME tends to $+\infty$ as any component $x_i \to \infty$. Hence $M(\delta_{ME,\lambda}, \epsilon) = +\infty$. In fact, ME is asymptotically not competitive even in the best case. Because of the fixed-point property of ME, $\delta_{ME,\lambda}(y) > e^{-1}$ if $y > e^{-1}$. Therefore, we immediately have

$$\inf_\lambda \inf_{X_n(\epsilon)} E\,\text{MSE}(\delta_{ME,\lambda}(y), x) > e^{-2}(1-\epsilon)\Phi(-(\sigma\, e)^{-1}),$$

which does not go to zero with ϵ. [2]

[2] By changing the "Default Value" A mentioned in the previous footnote, it is possible to improve the best case performance somewhat. However, the worst case performance does not improve.

In another direction, the minimax risk among linear procedures in this problem is precisely σ^2, for each $\epsilon > 0$: linear procedures are unable to take advantage of sparsity. Finally, the family of "threshold" estimators $\delta_{Thresh,\lambda}(y) = y1_{\{y \geq \lambda\}}$ has a minimax risk $\inf_\lambda M(\delta_{Thresh,\lambda}, \epsilon)$ which goes to zero with ϵ, but at a rate slightly worse than that indicated for the l_1 method.

2.3 Bias versus Variance

The risk improvements attained by the nonlinear methods above come at price: the estimators are biased. This may be seen by comparison of Figures 2.2a and 2.2c. All the zero values in Panel a are estimated in Panel c by positive values offset from zero by a nearly constant displacement. The peak values in Panel a are estimated in Panel c by systematically smaller $\hat{x}$. Such 'Amplitude Bias' is present also for the l_1 estimate. This bias is of course necessary in order to obtain the risk savings. The unbiased estimate $\hat{x} = y$ has expected mean squared error σ^2, which is much larger.

3 Applications to Spectroscopy

The results of the previous section have a broader significance than one might at first suppose. Suppose that instead of observations (4) we have observations according to the original model (1), with linear operator K an *orthogonal matrix*. Such K arise in Hadamard transform spectroscopy [14] where they are Hadamard matrices.

With K orthogonal, K^{-1} exists, and we can define pseudo-data $\tilde{y} = K^{-1}y$. As K preserves Euclidean distances, $||y - Kx||_2^2 = ||\tilde{y} - x||_2^2$. The general optimization problem (3) can be written as

$$\min_x \sum(\tilde{y}_i - x_i)^2 + 2\lambda \sum_i x_i \log x_i. \tag{11}$$

This is the same as the optimization problem (5) we encountered in the signal-plus-noise situation, only with pseudo-data $\tilde{y}$ replacing y. It follows that the solution to the ME problem is given simply by

$$\hat{x}_i = \delta_{ME,\lambda}(\tilde{y}_i) \;\; i = 1, \ldots, n. \tag{12}$$

A related analysis applies in NMR spectroscopy. In that area, when relaxation times and observation times are long, so that 'peak deconvolution' is not required [10], K may be modelled as the complex n by n discrete Fourier transform matrix. The data y and the object x to be recovered are then, in general, complex. It is possible to define an entropy for complex objects in several ways, and this leads to different properties of estimates; see [15]. We mention here the simplest definition, which leads to

$$\min_x ||y - Kx||_2^2 + 2\lambda \sum_i |x_i| \log |x_i|, \tag{13}$$

where, in this equation, $|z|$ denotes the modulus $(z\overline{z})^{1/2}$ of the complex number z. Now, the discrete Fourier transform matrix is, up to a constant factor, unitary; defining pseudo data $\tilde{y} = K^{-1}y$,

it turns out, by repeating earlier arguments, that $\hat{x}_i = \delta_{CME,\lambda}(\tilde{y}_i)$, for a certain 'complex ME' nonlinearity closely related to the 'real ME' nonlinearity.

There is a compact verbal description of the process of solving for x in (13). One first takes the inverse discrete Fourier transform of the observations y, getting pseudo data $\tilde{y}$, then one applies a complex-data ME nonlinearity coordinatewise. In contrast, conventional NMR spectroscopy consists in simply taking the inverse discrete Fourier transform of the data, and using the pseudo data $\tilde{y}$ to estimate x.

Hence in one area of NMR spectroscopy ('without deconvolution of line widths') the difference between conventional and ME restoration is simply in the application of a coordinatewise nonlinearity. We have conducted experiments to show this. Figure 3.1 presents three versions of the real part of an NMR spectrum of the compound tryptophan in D_2O at 400 MHz, taken on the JEOL GX-400 NMR spectrometer at the Rowland Institute, Cambridge, Mass. Figure 3.1a was prepared using standard Fourier transform methodology. Figure 3.1b was prepared using the Cambridge Maximum Entropy program [22] [24] using the four channel method for treating complex spectra, with "Default Value" parameter $A = .01$ and "Noise Level" parameter $S^2 = 5.1 \times 10^4$ (these parameters are called def and C_0 in the software documentation). Figure 3.1c was prepared using the idea described in [15,8]: computing the discrete Fourier transform, followed by a coordinatewise application of a 'complex ME' nonlinearity. In principle, figures 3.1b and 3.1c must be identical. Actually, they agree only to 6 digits of accuracy; this is due to the approximate, iterative nature of the numerical computations involved.

It is interesting to review Figure 1.1, taken from [22], with the developments of this section in mind. Visual comparison between Panels a, b, and c of this figure and the corresponding panels of Figure 2.2 or 3.1 leaves little doubt that the same effect which is achieved in Figure 1.1 by ME reconstruction could also be obtained by simply applying the right nonlinearity coordinatewise

to Panel a. In other words, the qualitative effect of using ME can, in this case, be obtained by a simple nonlinearity. The theory of section 2 therefore gives an explanation how ME has been able to improve signal-to-noise ratio in the *Nature* article [22].

Let us recall our three points.

Point [I]: Nonlinearities can be used to improve the mean squared error of estimation when the true object is near zero in all but a small fraction of samples. However, as we saw in section 2.1, if the object to be reconstructed is not nearly black, little improvement will be obtained. In some practical cases the true NMR spectrum has a 'nonzero background level'; there we expect that MEM does little to improve the signal-to-noise ratio. Figure 3.2 gives a comparison of an ME reconstruction (3.2b) with a conventional FT NMR reconstruction (3.2a). The object to be recovered is well away from zero in a significant portion of the display. Note that the ME reconstruction is noticeably less 'noisy' in the areas of the figure where the values are small, but the two figures differ negligibly in 'noisiness' in those areas where the values are well away from zero.

Point [II]: if near-blackness is present, it is clear from the discussion of section 2.2 that other nonlinearities can exploit it as well. One could, for example, define a 'complex l_1' method as the solution to

$$\min_x ||y - Kx||_2^2 + 2\lambda \sum_i |x_i|.$$

with $|\cdot|$ again the modulus; compare [18]. Presumably, an analysis similar to section 2.3, would show that this method performs very well in the nearly-black, complex-valued case.

Point [III]: One may seriously question the extent to which a gain in mean squared error leads to a gain in insight. When the comments of this section apply, the difference between ME and conventional reconstruction amounts to presenting the same data on two different plotting scales. Suppose that one wanted to identify peaks that were 'statistically significant', by the simple device of drawing a horizontal line across the plot at the 95th percentile of the null distribution of the plotted quantity (here

null refers to the assumption that the true signal value at that sample is zero). The calculation of the height at which such a line should be drawn would differ, depending upon whether we were plotting $\tilde{y}_i$ or the ME reconstruction $\delta_\lambda(\tilde{y}_i)$, but the same i-coodinates would be identified as significant.

One might therefore maintain that ME improves *signal-to-noise ratio* (if the signal is nearly black) but does not improve *sensitivity* (i.e. ability to succesfully discriminate small amplitude signal from noise). Compare [10,23].

The bias in amplitude estimates produced by ME should also be mentioned. While the ME reconstruction may be close to the truth in mean square, its peak amplitudes are biased. (The habit, in papers such as [22], of suppressing axis labels on plots obscures this fact.) In contrast, by improving the experiment, one gets a better signal-to-noise ratio without introducing bias.

4 Super-Resolution

A full discussion of Phenomenon (B) would require considerable space, so we specialize. We suppose that we have data according to model (1), where the object is a vector of dimension n, and the operator K consists of the first m rows of the n by n Discrete Fourier transform matrix:

$$K_{ji} = \begin{cases} \frac{1}{\sqrt{n}} \cos(\frac{\pi(i-1)(j-1)}{n}) & j = 1, 3, \ldots, m \\ \frac{1}{\sqrt{n}} \sin(\frac{\pi(i-1)j}{n}) & j = 2, 4, \ldots, m-1 \end{cases}$$

Then the observations vector y is of dimension m, and the elements of y represent noisy observations of the m low-order Fourier coefficients of x. (Our definition requires that m be *odd*). This is a discrete model of diffraction-limited imaging; compare [11,1, 19,4].

As in many other inverse problems, here the operator K is of less than full rank. It has m nonzero singular values and a null space of dimension $n - m$. Consequently, analysis by least squares or regularized least squares faces certain limitations. The formula $\hat{x}_{RLS} = (K^T K + \lambda I)^{-1} K^T y$ gives an estimate $\hat{x}$ which must lie in a subspace of dimension m, consisting of those vectors x whose last $n - m$ Fourier coefficients vanish. Vectors whose high-order Fourier coefficients vanish are representable as sums of low frequency sinusoids, and are in a certain sense "smooth".

While there certainly exist applications where the object to be recovered is smooth, in areas like astronomy or spectroscopy the object to be recovered is nearly a set of scattered spikes. The smoothing effect of regularized least squares can be to lump two closely spaced spikes together into a single bump. Therefore, in such areas, regularized least squares can hide important structure. The terminology "Rayleigh distance" describes this effect; this is the minimal distance two spikes must be spaced apart so that they can still be visually recognized as separate features in the conventionally reconstructed image. The Rayleigh distance in this discrete model may be taken as $R = \frac{n}{m}$. This is the reciprocal of the *incompleteness ratio* $\epsilon = \frac{m}{n}$.

Frieden [11] demonstrated convincingly that ME can, sometimes, resolve structures closer together than the Rayleigh distance. This was illustrated in Figure 1.2.

4.1 Theory of Superresolution

Frieden's is not the only example of the superresolution phenomenon. There is by now a considerable literature documenting many different nonlinear algorithms which may be employed to obtain superresolution. Jansson's book [16] contains several articles detailing different approaches.

However, superresolution is not well-understood theoretically. To our knowledge, no theoretical treatment has emerged to answer questions such as: "If the Rayleigh limit can be circumvented by nonlinear procedures, what is the true limit of resolution?" The absence of a theory of superresolution makes it easy for skeptics to invoke general principles (e.g. "There's no such thing as a free lunch") which in their view, cast doubt on the whole superresolution phenomenon.

We have developed a theory which shows when superresolution is possible, and what its limits are. From empirical work reported in [9], we believe that the theory adequately models the application of superresolving methods to real data. In this paper, we present a limited selection of results. We hope to report at length on this theory elsewhere. Here and below we adopt the usual conventions $||v||_1 = \sum_i |v_i|$, $||v||_2 = \sqrt{\sum_i v_i^2}$, and $||v||_\infty = \max_i |v_i|$.

Definition. *Let*

$$\omega(\Delta; x) = \sup\{||x' - x||_1 : ||Kx' - Kx||_2 \leq \Delta \quad and \quad x' \geq 0\}. \tag{14}$$

We say that x admits of superresolution if

$$\omega(\Delta; x) \to 0 \quad as \ \Delta \to 0. \tag{15}$$

The definition makes sense. Suppose x admits superresolution according to our definition. When we observe data $y = Kx + z$,

and the noise z satisfies $||z||_2 \leq \Delta$, then if $\hat{x}$ is any purported reconstruction satisfying

$$||y - K\hat{x}||_2 \leq \gamma\Delta \tag{16}$$

and

$$\hat{x}_i \geq 0 \quad i = 1, \ldots, n, \tag{17}$$

we must have, by the triangle inequality,

$$||\hat{x} - x||_1 \leq \omega((1+\gamma)\Delta; x). \tag{18}$$

If the noise level Δ is small enough, this means that $\hat{x}$ accurately reconstructs x from the partial information $y = Kx + z$.

Examples of methods satisfying (16)-(17) are Maximum Entropy in constrained form (2), with $S = \gamma\Delta$, or the minimum l_1 variant, defined by

$$\min \sum_i x_i \qquad \text{subject to } ||y - Kx||_2 \leq S$$
$$\text{and} \quad x \geq 0$$

also with $S = \gamma\Delta$. One could also mention the positive-constrained least-squares estimate, defined by

$$\min ||y - Kx||_2 \quad \text{subject to} \quad x \geq 0,$$

which satisfies (17) and (16) with $\gamma = 1$.

On the other hand, suppose that x does not admit superresolution, as we have defined it. Then, there exists x' which is nonnegative and unequal to x, yet $Kx' = Kx$. Even with noiseless data, we cannot say whether x or x' is the true object. Other pathologies occur in this case; one can show that neither the minimum l_1 estimate nor the positivity-constrained least-squares estimate is uniquely-defined for small noise levels, etc.

Our definition is particularly strong, intended to convince skeptics rather than reassure advocates. In fact, the definition is so strong that it may be surprising that there is any x which admits of superresolution. Under this definition, x must be so

special that any method – ME, or any of those described in [16] – must give a good restoration of the full object x, from incomplete, noisy data y if the noise level Δ is small, and if the restoration method obeys (16)-(17).

In fact, all sufficiently nearly black objects admit of superresolution, as we see in Theorem 3 below.

A certain geometry underlies the definition: see Figure 4.1. When (16)-(17) hold, we know from the triangle inequality that $||K(x' - x)|| \leq (1 + \gamma)\Delta$. For the particular K we are using, the set of all possible reconstructions x' obeying this inequality is a cylinder, the product of an m-dimensional sphere with an $n - m$-dimensional affine subspace. This set of reconstructions is unbounded. However, when we include the constraint that we are interested only in positive reconstructions, attention focuses on the small cross-hatched area in the figure. When we are lucky enough that the geometry of the situation is as in that figure, the set of all possible reconstructions is small, and also its diameter tends to zero as $\Delta \rightarrow 0$.

The issue, of course, is to find for which x the geometry is of the favorable kind indicated by the figure. The following, basically technical result, permits a reduction.

Theorem 2 *x admits of superresolution if and only if there exists a finite, positive constant C so that*

$$||x' - x||_1 \leq C\,||Kx' - Kx||_2 \tag{19}$$

holds whenever

$$x'_i \geq 0 \quad i = 1, \ldots, n. \tag{20}$$

Let $C(K, x)$ denote the smallest constant for which (19)-(20) hold, and $C(K, x) = \infty$ if no such relations hold. If $C < \infty$, x admits superresolution, and

$$\omega(\Delta; x) \sim C(K, x)\,\Delta \quad as \quad \Delta \rightarrow 0. \tag{21}$$

We therefore turn attention to the coefficient $C(K, x)$. It is clear from the proof of Theorem 2 that $C(K, x)$ does not depend

on x except through the number and arrangement of nonzero elements – i.e. the amplitudes of the nonzero elements don't matter. Our main result involves just the number of nonzero elements:

Theorem 3 *(1) If x has $\frac{m-1}{2}$ or fewer nonzero elements then $C(K,x) < \infty$.*

(2) If $\frac{m+1}{2}$ divides n, there exists x with $\frac{m+1}{2}$ nonzero elements yet $C(K,x) = \infty$.

(3) If x has more than m nonzero elements then $C(K,x) = \infty$.

The proof, in section 6, revolves around a lower bound on the number of negative values taken on by high-frequency sequences. B.F. Logan [17] introduced a method for constructing low-frequency functions with prescribed zeros. By adapting his method to construct low-frequency sequences with prescribed sign patterns, we are able to get the required lower bound.

We restate the result in the language of our title. If the incompleteness ratio is $\epsilon = m/n$, *x must admit superresolution if x is $\epsilon/2$-black.* Moreover, *x might not admit superresolution if x is not $\epsilon/2$-black* and *x cannot admit superresolution if x is not ϵ-black.*

Thus, near blackness is both necessary and sufficient for superresolution.

We now briefly turn to consider the size of C. Obviously, when C happens to be very large, say 10^{12}, superresolution is largely a theoretical curiosity, since sub-quantum noise levels would be required to make $C\,(1+\gamma)\,\Delta$ small enough to exert useful control on the reconstruction error $||\hat{x} - x||_1$.

It turns out that C is strongly correlated with the *spacing* of nonzero elements in x. If all nonzero elements in x are well-spaced, then C can be moderately small; but if it can happen that as many as r are bunched together within a Rayleigh interval, then C can be very large, growing roughly exponentially in r.

Theorem 4 *There exists x having only r nonzero elements, and a nonnegative x' such that*

$$||x' - x||_1 = \Gamma(r, m, n)\, ||K(\hat{x} - x)||_2 \tag{22}$$

where, if $m, n \to \infty$ with r fixed, and $m/n \to \epsilon$,

$$\Gamma(r, m, n)^{-2} \sim \frac{1}{2\pi} \int_0^{\pi\epsilon} |P_r(\theta)|^2 d\theta, \tag{23}$$

where P_r is a certain trigonometric polynomial having $P_r(\theta) \sim (\theta/2)^{2r}$ as $\theta \to 0$. In particular, for small ϵ,

$$\Gamma(r, m, n) \approx \sqrt{8r + 2}\, \pi^{-2r}\, (\epsilon/2)^{-2r-1/2}. \tag{24}$$

4.2 Interpretation

Our three claims of the introduction apply to this phenomenon also.

[I] *Superresolution is a real, delicate, nonlinear effect.* It is *real*, because we have proved that under certain conditions, ME accurately reconstructs the unknown object, despite massive incompleteness. It is *delicate*, because it depends on the near-blackness of the object to be reconstructed (by Theorem 3). It is *nonlinear*, because it depends on the two properties (16)-(17); these cannot both be guaranteed by linear methods.

[II] *ME is not the only method which exhibits superresolution.* As mentioned earlier, many different methods have been shown to exhibit it in published examples. In our theory, any method with the two properties (16)-(17) exhibits superresolution.

[III] *Superresolution produced by these nonlinear methods is not, in general, a substitute for superresolution produced by developing better instrumentation (i.e. increasing m).* If the object to be recovered consists of a few spikes spaced well apart, the coefficient C can be moderate in size, and ME and like methods might conceivably give a highly accurate reconstruction. But if there are a number of spikes close together, Theorem 4 shows that

the coefficient C can be very large, and the prospects for accurate reconstruction are doubtful. In contrast, developing better instrumentation would increase the resolution of the experiment for both the easy (well-spaced) cases, and the hard ones.

5 Summary

ME is a nonlinear inversion technique which sometimes exhibits two desirable phenomena

- (A) Signal-to-Noise enhancement beyond what linear methods can achieve.
- (B) Resolution of spikes spaced more closely together than the resolution limit for linear techniques.

Proponents of ME have performed a service to inverse theorists by demonstrating the possibility of these phenomena, and to practitioners by making available efficient ME software which makes it possible to exploit these phenomena.

This paper is being written against a background of some controversy [25,26,23]. Some ME advocates have, in highly visible fora, claimed explicitly that ME is the one and only method to use for solving inverse problems where the answer is known to be positive. For the record, our philosophy is:

> *Names don't matter; performance does. The fact that the ME penalty functional can be called "entropy" is irrelevant. The fact that entropy has a distinguished patrimony (Boltzmann, Gibbs, Shannon) is irrelevant. The fact that entropy has useful applications in unrelated areas (coding theory) is irrelevant. The fact that entropy satisfies simple functional equations is irrelevant. It does matter how ME reconstruction* **performs** *in the problem at hand, and that it sometimes uncovers surprising phenomena. It does matter to* **explain** *those surprises, why they occur, and when they* **do** *and* **do not** *occur.*

In certain 'fundamentalist ME' quarters, we could expect violent disagreement with each phrase in the above credo. On the other hand, one of the originators of ME inversion is B.R. Frieden,

who is distinctly not of the fundamentalist sect. Alone among ME advocates, he has evidenced concern for describing the properties of signal and noise that lead ME to improve significantly upon conventional methods [11], and for describing conditions under which ME *fails* to improve upon conventional methods [12]. We interpret his work as precursor of our points [I]-[III], and believe that it lends independent support to our conclusions. He might even agree with our credo.

6 Proofs

6.1 Proof of Theorem 1

The arguments presented here are related to those in [7], where a fuller account, for a different class of parameter spaces, may be found. The reader is urged to consult that paper to clarify any issues that arise in the understanding of the proofs. The reader may also be helped for section 6.1.1 by consulting [20] and for section 6.1.2 by consulting [5].

6.1.1 Proof of Formula for $M(\epsilon)$

Let Π_G denote the set of exchangeable probability measures on R^n which put mass 1 on $X_n(\epsilon)$. For a measure π on R^n, define the Bayes Risk

$$\rho(\pi) = n^{-1}\mathrm{E}\,||\mathrm{E}\,\{x|y\} - x||_2^2.$$

As in [7], the minimax theorem of decision theory implies that

$$M_n(\epsilon) = \sup\{\rho(\pi) : \pi \in \Pi_G\}. \tag{25}$$

Given $\pi \in \Pi_G$ let π_0 be the product measure with the same marginal. As in [7] we have $\rho(\pi) \leq \rho(\pi_0)$. Now if we define the rescaled marginal $F_{1,\sigma} = \pi\{x_1/\sigma \leq t\}$, the Bayes risk $\rho(\pi_0) = \sigma^2(1 - I(F_{1,\sigma} * \Phi))$, where Φ denotes the standard univariate Gaussian distribution, and I denotes the Fisher Information (this is an identity due to L.D. Brown; see for example [7,5]). Finally observe that $\{F_{1,\sigma} : \pi \in \Pi_G\} = \mathcal{F}_\epsilon$. Combining these facts,

$$M_n(\epsilon) \leq \sigma^2(1 - \inf\{I(F * \Phi) : F \in \mathcal{F}_\epsilon\})$$

for every n, so that

$$M(\epsilon) \leq \sigma^2(1 - \inf\{I(F * \Phi) : F \in \mathcal{F}_\epsilon\}) \tag{26}$$

Let $\alpha < \epsilon$. There exists a sequence $(F_{k,\alpha}, k = 1, 2, \ldots)$ of distributions in $\mathcal{F}_\alpha$ with

$$I(F_{k,\alpha} * \Phi) \to \inf\{I(F * \Phi) : F \in \mathcal{F}_\alpha\}$$

and, additionally, Support$(F_{k,\alpha}) \subset [0,k]$.

Put $A_n = \{x \in X_n(\epsilon)\}$. Let π_0 be product measure with marginal $F_{k,\alpha}$. Let $Bin(n,p)$ denote a random variable with binomial distribution having parameters n and p. Then

$$\pi_0(A_n) \geq P\{Bin(n,\alpha) \leq n\epsilon\} \rightarrow 1 \tag{27}$$

as $n \rightarrow \infty$. Define the conditional measure $\pi_n(B) = \pi_0(B|A_n)$. Then $\pi_n \in \Pi_G$, and so by (25), $M_n(\epsilon) \geq \rho(\pi_n)$. Lemma 1 below shows that π_n is so close to π_0 that

$$\frac{\rho(\pi_n)}{\rho(\pi_0)} \rightarrow 1 \tag{28}$$

as $n \rightarrow \infty$. As $\rho(\pi_0) = \sigma^2(1 - I(F_{k,\alpha} * \Phi))$, we then have

$$\liminf_{n\rightarrow\infty} M_n(\epsilon) \geq \sigma^2(1 - I(F_{k,\alpha} * \Phi)).$$

As $M(\epsilon) \geq M_n(\epsilon)$, it follows upon letting $k \rightarrow \infty$ that

$$M(\epsilon) \geq \sigma^2(1 - \inf\{I(F * \Phi) : F \in \mathcal{F}_\alpha\}).$$

Now $I(F * \Phi)$ is a continuous functional of F in supremum norm (compare, for example, [6]); letting $\alpha \rightarrow \epsilon$ and invoking this continuity, we get the reverse inequality to (26), and (8) follows.

Lemma 1 *Eq. (28) holds.*

Proof. We note that

$$\begin{aligned} \mathrm{E}_{\pi_0}\{x|y\} &= \pi_0(A_n)\mathrm{E}_{\pi_0}\{x|y,A_n\} + \pi_0(A_n^c)\mathrm{E}_{\pi_0}\{x|y,A_n^c\} \\ &= \pi_0(A_n)\mathrm{E}_{\pi_n}\{x|y\} + \pi_0(A_n^c)\mathrm{E}_{\pi_0}\{x|y,A_n^c\}. \end{aligned}$$

As Support$(\pi_0) \subset [0,k]^n$, both $\mathrm{E}_{\pi_0}\{x|y,A_n\}$ and $E_{\pi_0}\{x|y,A_n^c\}$ belong to $[0,k]^n$ for every y, and

$$\begin{aligned} & ||\mathrm{E}_{\pi_n}\{x|y\} - \mathrm{E}_{\pi_0}\{x|y\}||_2^2 \\ = \; & (1 - \pi_0(A_n))^2 ||E_{\pi_0}\{x|y,A_n\} - E_{\pi_0}\{x|y,A_n^c\}||_2^2 \\ \leq \; & nk^2(1 - \pi_0(A_n))^2 \end{aligned}$$

Now let μ denote the joint distribution of (x, y) when $x \sim \pi_n$, and $y \sim N(x, \sigma^2 I)$. Then

$$n^{-1} \mathrm{E}_{\mu} ||\mathrm{E}_{\pi_0}\{x|y\} - x||_2^2 \geq (\rho(\pi_0) - (1 - \pi_0(A_n))k^2)/\pi_0(A_n) \to \rho(\pi_0).$$

and

$$\begin{aligned} \rho(\pi_n) &= n^{-1} \mathrm{E}_{\mu} ||E_{\pi_n}\{x|y\} - x||_2^2 \\ &\geq n^{-1} \mathrm{E}_{\mu} ||E_{\pi_0}\{x|y\} - x||_2^2 - B_n/n \end{aligned}$$

with

$$B_n^2 = 4 \, \mathrm{E}_{\mu} ||E_{\pi_0}\{x|y\} - x||_2^2 \, \mathrm{E}_{\mu} ||E_{\pi_0}\{x|y\} - E_{\pi_n}\{x|y\}||_2^2 = o(n^2).$$

Combining these inequalities with the definition of $\rho(\pi_n)$ and with (27) gives (28).

6.1.2 Asymptotic Formula for $M(\epsilon)$

In this subsection, we establish the lower bound

$$M(\epsilon) \geq 2\sigma^2 \, \epsilon \log(\epsilon^{-1})(1 + o(1)). \tag{29}$$

The upper bound on behavior of the l_1 rule of the next subsection shows that equality holds. Here and in the next section we take $\sigma = 1$, without any loss of generality. (29) follows from (8), taking a large in (31) below.

Proposition 1 *Let $F_{\epsilon,\mu} = (1-\epsilon)\nu_0 + \epsilon\nu_\mu$, where ν_x denotes Dirac Mass at x. Let $a > 0$, and, for all sufficiently small ϵ, define μ implicitly as a function of ϵ by*

$$\mu^2 + 2a\mu = 2\log(\epsilon^{-1}). \tag{30}$$

Then

$$1 - I(\Phi * F_{\epsilon,\mu}) \sim \epsilon\mu^2\Phi(a) \quad \text{as } \epsilon \to 0. \tag{31}$$

Proof. By L.D. Brown's identity, $1 - I(\Phi * F_{\epsilon,\mu})$ is the Bayes risk for estimation of the 1-dimensional parameter θ from data which is $N(\theta, 1)$, when θ is 0 with probability $(1-\epsilon)$, and μ with probability ϵ.

This risk may be written

$$\rho = (1-\epsilon)\int(\mathrm{E}\,\{\theta|y\} - 0)^2\phi(y)dy + \epsilon\int(\mathrm{E}\,\{\theta|y\} - \mu)^2\phi(y-\mu)dy$$

Define $p(y) = P\{\theta = \mu|y\}$, and note that

$$\mathrm{E}\,\{\theta|y\} = \mu p(y).$$

Lemma 2 below shows that as $\epsilon \to 0$, p tends to zero or one depending on whether y is smaller than or bigger than $\mu + a$. Applying this, and carefully bounding remainder terms,

$$\rho = (1-\epsilon)\mu^2\int_{\mu+a}^{\infty}\phi(y)dy + \epsilon\mu^2\int_{\infty}^{\mu+a}\phi(y-\mu)dy + o(\epsilon\mu^2) \quad (32)$$

Now using the assumption (30)

$$\phi(\mu + a) = \phi(0)\epsilon\exp(-a^2)$$

and the standard inequality

$$1 - \Phi(t) \le \frac{\phi(t)}{t} \quad \text{for all } t \ge 1 \quad (33)$$

we get

$$(1-\epsilon)\mu^2\int_{\mu+a}^{\infty}\phi(y)dy = O(\epsilon\mu) = o(\epsilon\mu^2),$$

and so the first term in (32) is negligible compared with the second term, leaving

$$\rho \sim \epsilon\mu^2\Phi(a)$$

as required.

Lemma 2 *With the assumptions and notation of Proposition 1,*

$$p(\mu + z) \to \begin{cases} 1 & z > a \\ 0 & z < a \end{cases}, \quad (34)$$

as $\epsilon \to 0$, *uniformly in* $z > a + \delta$ *and in* $z < a - \delta$, $\delta > 0$.

Proof.

$$p(y) = \frac{\epsilon\phi(y-\mu)}{(1-\epsilon)\phi(y) + \epsilon\phi(y-\mu)}$$

so that

$$p(\mu+z) = \left((1-\epsilon)\exp\{-\mu z - \mu^2/2 + \log(\epsilon^{-1})\} + 1\right)^{-1}.$$

Now by (30) $-\mu^2/2 + \log(\epsilon^{-1}) = a\mu$, so

$$p(\mu+z) = ((1-\epsilon)\exp\{\mu(a-z)\} + 1)^{-1}.$$

From this, (34) is immediate.

6.1.3 Asymptotic Minimaxity of the l_1 rule

We complete the proof of (9) and (10) by showing that if we put

$$\lambda^2 = 2\log(\epsilon^{-1}) \tag{35}$$

then, for the l_1 rule δ_n based on this choice of λ, we have

$$\sup_n M_n(\delta_n, \epsilon) \le \lambda^2\epsilon\,(1 + o(1)) \quad \text{as } \epsilon \to 0 \tag{36}$$

Since the μ of last section and λ of this section are asymptotically equivalent, this shows that the inequality in (29) can be replaced by equality. It also shows that the choice (35) is asymptotically optimal. Letting $\delta(y) = \max(0, y-\lambda)$, we have

$$\text{E MSE}(\delta_n, x) = \int\int (\delta(\theta+z) - \theta)^2\,\phi(z)dz\,dF_n(\theta)$$

where F_n is the empirical distribution of the x_i. As this functional is linear in F_n, and as $F_n(0) \ge (1-\epsilon)$ whenever $x \in X_n(\epsilon)$, we have

$$\text{E MSE}(\delta_n, x) \le (1-\epsilon)r(\lambda, 0) + \epsilon \sup_\mu r(\lambda, \mu)$$

where

$$r(\lambda, \mu) \equiv \text{E}\,(\delta(\mu+z) - \mu)^2.$$

A calculation gives

$$r(\lambda,\mu) = \mu^2\Phi(\lambda-\mu) - (\lambda+\mu)\phi(\lambda-\mu) + (\lambda^2+1)(1-\Phi(\lambda-\mu)).$$

This implies

$$\frac{\partial}{\partial\mu} r(\lambda,\mu) = 2\mu\Phi(\lambda-\mu),$$

and so

$$\sup_{\mu} r(\lambda,\mu) = r(\lambda,+\infty) = (\lambda^2+1).$$

Moreover,

$$r(\lambda,0) = -\lambda\phi(\lambda) + (\lambda^2+1)(1-\Phi(\lambda)).$$

By (35) we have

$$\phi(\lambda) = \phi(0)\epsilon;$$

using again (33), we get $(1-\Phi(\lambda)) \leq \phi(0)\epsilon/\lambda$ and so

$$r(\lambda,0) \leq \frac{\epsilon\phi(0)}{\lambda}.$$

We conclude that for $\epsilon < e^{-1}$,

$$(1-\epsilon)r(\lambda,0) + \epsilon r(\lambda,\mu) < \epsilon(\lambda^2+2)$$

and (36) follows.

6.2 Proof of Theorem 2

Let $\mathcal{Z} = \{i : x_i = 0\}$. Let $\mathcal{V} = \{v : ||v||_1 = 1 \quad \text{and} \quad v_i \geq 0, i \in \mathcal{Z}\}$. Then $\mathcal{V}$ is closed and compact. Let v^* be any minimizer of $||Kv||_2$ on $\mathcal{V}$.

If $||Kv^*||_2 > 0$, we claim that $C = 1/||Kv^*||_2$, and that $\omega(\Delta;x) = C\Delta$ for small enough Δ. If $||Kv^*||_2 = 0$, we claim that $C = \infty$ and that $\omega \not\to 0$. These two claims together prove the Theorem.

Assume that $||Kv^*||_2 > 0$. Put $v = x' - x$, $x' \geq 0$. Then $v/||v||_1 \in \mathcal{V}$, so

$$||Kv||_2 \geq ||Kv^*||_2||v||_1;$$

Hence $C \leq 1/||Kv^*||_2$.

Now, if we pick α very small, then $x' = x + \alpha v^*$ defines a nonnegative vector, with

$$||K(x' - x)||_2 = \alpha||Kv^*||_2 = ||Kv^*||_2||x' - x||_1$$

so

$$\omega(\Delta; x) \geq \alpha||v^*||_1 \quad \text{for } \Delta > \alpha||Kv^*||_2 \tag{37}$$

for all $\alpha \leq \alpha_0$, say. As $||Kv^*||_2 > 0$, this says

$$\omega(\Delta; x) \geq \Delta/||Kv^*||_2$$

for $\Delta < \Delta_0$. By definition of ω and C,

$$\omega(\Delta; x) \leq C(K, x)\Delta, \quad \Delta > 0.$$

It follows that $C \geq 1/||Kv^*||_2$, and hence $C = 1/||Kv^*||_2$. We may also conclude that

$$\omega(\Delta; x) = C(K, x)\Delta, \quad \Delta < \Delta_0,$$

completing our first claim.

For the second claim, suppose $||Kv^*||_2 = 0$. Let α_0 be any positive value of α for which (37) holds. Then

$$\liminf_{\Delta \to 0} \omega(\Delta; x) \geq \alpha_0.$$

I.e., $\omega \not\to 0$ as $\Delta \to 0$. From this and (38), $C = \infty$, completing the proof of the second claim.

6.3 Proof of Theorem 3

Assertion (3) of the theorem is an exercise in parameter counting and linear algebra. We omit the argument.

Let $0 \leq k < n/2$. $\mathcal{B}(k)$ is the set of *discrete bandlimited sequences* of length n and bandwidth k, i.e. the real sequences (b_i) satisfying

$$\sum_{i=1}^{n} b_i \exp\{\sqrt{-1}\frac{2\pi(i-1)j}{n}\} = 0 \quad j = k+1, \ldots, n-1-k.$$

Let $1 < l < n/2$. $\mathcal{H}(l)$ is the set of *discrete highpass sequences* of length n, i.e. the real sequences (h_i) satisfying

$$\sum_{i=1}^{n} h_i \exp\{\sqrt{-1}\frac{2\pi(i-1)j}{n}\} = 0 \quad j = 0, \ldots, l-1, n-l+1, \ldots, n-1.$$

It follows from Parseval's relation for the finite Discrete Fourier transform that if $b \in \mathcal{B}(k)$ and $h \in \mathcal{H}(l)$, with $k < l$, then

$$\sum_i b_i h_i = 0. \tag{39}$$

The importance of these two vector spaces is that

$$\mathcal{B}(\frac{m-1}{2}) = Range(K^T K); \quad \mathcal{H}(\frac{m+1}{2}) = Kernel(K^T K).$$

Let $\mathcal{Z} = \{i : x_i > 0\}$. From the proof of Theorem 2 we know that $C(K, x) = \infty$ iff there exists $v \neq 0$ such that $Kv = 0$ yet $v_i \geq 0, i \in \mathcal{Z}$. From now on we fix $l = \frac{m+1}{2}$. We can rephrase the condition of Theorem 2 as

$$C(K, x) = \infty \quad \text{iff for some nonzero} \quad h \in H(l), h_i \geq 0, \quad i \in \mathcal{Z}. \tag{40}$$

We use this to prove the two halves of the Theorem.

6.3.1 (1): Fewer than $\frac{m}{2}$ Nonzero Elements

The lemma below shows that a nonzero $h \in \mathcal{H}(l)$ has at least l negative elements. For such an h to satisfy $h_i \geq 0$, $i \in \mathcal{Z}$, we must have $Card(\mathcal{Z}) \leq n - l$, i.e. x has at least l nonzero elements. As $l > \frac{m}{2}$ this cannot happen. The proof of the first half is complete.

Lemma 3 *Let $h \in \mathcal{H}(l)$. If $h \neq 0$, then h has at least l negative elements.*

Proof. Put $\mathcal{P} = \{i : h_i \geq 0\}$. Put $k = Card(\mathcal{P}^c)$. We claim there exists a sequence $b = (b_i)$ so that

$$\min_i |b_i| > 0, \tag{41}$$

$$b_i h_i \geq 0, \quad i = 1, \ldots, n, \tag{42}$$

and

$$b \in \mathcal{B}(k). \tag{43}$$

It follows from (41)-(42) that

$$\sum_i b_i h_i \geq \min_i |b_i| \sum_i |h_i|.$$

Now if $k < l$, $\mathcal{H}(k+1) \supseteq \mathcal{H}(l)$. Therefore $\mathcal{B}(k)$ and $\mathcal{H}(l)$ are orthogonal. It follows that $\sum_i b_i h_i = 0$, which forces $h = 0$. Consequently, if $k < l$ then $h = 0$.

The construction of such a b is made by adapting a construction of B.F. Logan, who used it to show that continuous-time high-pass functions must change sign frequently [17, Theorem 5.2].

Let $(i_u)_{u=1}^k$ be an enumeration of the elements of $\mathcal{P}^c$. Define

$$s_u = \frac{2\pi(i_u - 1/2)}{n} \tag{44}$$

$$t_u = \frac{2\pi(i_u + 1/2)}{n} \tag{45}$$

for $u = 1, \ldots, k$. Define the sequence

$$b_i^{(u)} = \sin(\frac{1}{2}(\frac{2\pi i}{n} - s_u)) \sin(\frac{1}{2}(\frac{2\pi i}{n} - t_u)). \tag{46}$$

The reader will want to check at this point that

$$\begin{aligned} b_i^{(u)} &> 0, \quad i \in \{1, \ldots, n\} - \{i_u\} \\ b_i^{(u)} &< 0, \quad i = i_u. \end{aligned} \tag{47}$$

Now putting (46) in the equivalent form

$$b_i^{(u)} = [\cos(\frac{\pi}{n}) - \cos(\frac{2\pi}{n}(i - i_u))]/2,$$

shows that, for certain constants $e_0^{(u)}$, $e_1^{(u)}$, and $f_1^{(u)}$, we have

$$b_i^{(u)} = e_0^{(u)} + e_1^{(u)} \cos(\frac{2\pi(i-1)}{n}) + f_1^{(u)} \sin(\frac{2\pi(i-1)}{n}). \tag{48}$$

In other words, $b^{(u)} \in \mathcal{B}(1)$. Define now

$$b_i = (-1)\,\Pi_{u=1}^{k} b_i^{(u)} \tag{49}$$

this gives a sequence (b_i) such that

$$b_i > 0, \quad i \in \mathcal{P}$$

$$b_i < 0, \quad i \in \mathcal{P}^c.$$

Properties (41)-(42) follow. By the Convolution Theorem for the finite discrete Fourier transform, one may show that if $b^{(1)}, \ldots, b^{(k)}$ are all in $\mathcal{B}(a)$, then $\Pi_{u=1}^{k} b^{(u)}$ is in $\mathcal{B}(ka)$. As the $b^{(u)}$ are all in $\mathcal{B}(1)$ we conclude that (43) holds.

One could also check this directly by combining (48) with (49), giving explicitly the representation

$$b_i = e_0 + \sum_{u=1}^{k} e_u \cos(\frac{2\pi(i-1)u}{n}) + f_u \sin(\frac{2\pi(i-1)u}{n}),$$

which implies (43).

6.3.2 (2): More than $\frac{m}{2}$ Nonzero Elements

By hypothesis, l divides n. Pick $0 < t < \frac{n}{l}$, and define

$$h_i = \begin{cases} 1 & i = 0, \frac{n}{l}, 2\frac{n}{l}, \ldots \\ -1 & i = t, t + \frac{n}{l}, t + 2\frac{n}{l}, \ldots \\ 0 & else \end{cases}$$

Now (h_i) is periodic with period $\frac{n}{l}$. Thus h is representable as a Fourier sum using only sinusoids also of period $\frac{n}{l}$. Hence

$$\sum_{i=1}^{n} h_i \exp\{\frac{2\pi(i-1)j}{n}\} = 0, \quad j \notin \{0, l, 2l, \ldots, n-l\}.$$

Now by construction $\sum_i h_i = 0$. Hence,

$$\sum_{i=1}^{n} h_i \exp\{\frac{2\pi(i-1)j}{n}\} = 0, \quad j \notin \{l, 2l, \ldots, n-l\};$$

which implies $h \in \mathcal{H}(l)$.

If we define

$$x_i = \begin{cases} 1 & i = t, t + \frac{n}{l}, t + 2\frac{n}{l}, \ldots \\ 0 & else \end{cases},$$

then x_i has only l nonzero elements. Putting $\mathcal{Z} = \{i : x_i = 0\}$, we see that $h_i \geq 0$, $i \in \mathcal{Z}$. Hence, (40) is satisfied for this h and this x, and $C(K, x) = \infty$.

6.4 Proof of Theorem 4

We treat indices circularly, so that 0 is identified with n, -1 with $n-1$, etc. Put $u = r - 1$.

Suppose that r is odd. Let $x_i = 1$ if $i = -u, u+2, \ldots, -2, 0, 2, \ldots, u-2, u$, and $x_i = 0$, otherwise.

If, instead, r is even, let $x_i = 1$ if $i = -u, u+2, \ldots, -1, 1, \ldots, u-2, u$, and $x_i = 0$, otherwise.

Define the sequence $c = (c_i)_{i=1}^n$ via

$$c_i = \begin{cases} (-1)^i \begin{pmatrix} 2r \\ r+i \end{pmatrix} 2^{-2r} & -r \leq i \leq r \\ 0 & \text{else} \end{cases}$$

Pick $\alpha > 0$ with

$$\alpha < \min_{-r \leq i \leq r} 1/|c_i|.$$

Define x' by

$$x'_i = x_i + (-1)^r \alpha c_i \quad i = 1, \ldots, n;$$

then $x' \geq 0$. Now

$$||x' - x||_1 = \alpha \sum_i |c_i| = \alpha$$

and

$$||K(x' - x)||_2 = \alpha \, (\sum_{j=1}^{m} (\hat{c}_j)^2)^{1/2}$$

where

$$\hat{c}_j = \begin{cases} \frac{1}{\sqrt{n}} \sum_i c_i \cos(\frac{\pi i(j-1)}{n}) & j = 1, 3, 5, \ldots, m \\ \frac{1}{\sqrt{n}} \sum_i c_i \sin(\frac{\pi ij}{n}) & j = 2, 4, 6, \ldots, m-1 \end{cases}$$

are the discrete Fourier coefficients of c. Note that c is an even sequence, so that the sine coefficients vanish: $\hat{c}_j = 0$, $j = 2, 4, 6, \ldots$.

Define now $P_r(\theta) = \sum_{i=-r}^{r} c_i \cos(\theta i)$, so that $\hat{c}_j = \frac{1}{\sqrt{n}} P_r(\frac{\pi(j-1)}{n})$ for $j = 1, 3, 5, \ldots$. With this notation, (22) holds, with

$$\Gamma(r, m, n)^{-2} = \sum (\hat{c}_j)^2 = n^{-1} \sum_{0 \le j < m/2} |P_r(\frac{2\pi j}{n})|^2. \qquad (50)$$

As P_r is Riemann integrable, if we let $n, m \to \infty$ with $m/n \to \epsilon \in (0, 1)$,

$$n^{-1} \sum_{0 \le j < m/2} |P_r(\frac{2\pi j}{n})|^2 \to \frac{1}{2\pi} \int_0^{\pi\epsilon} |P_r(\theta)|^2 d\theta.$$

To estimate the behavior of P_r, let f denote a function defined on the real line. Define the $2r$-th order differencing operator

$$(\Delta_h^{2r} f)(x) = \sum_{i=-r}^{r} (-1)^i \binom{2r}{r+i} f(x + hi).$$

Then if f is integrable

$$2^{2r} P_r(\theta) \hat{f}(\theta) = (\widehat{\Delta_1^{2r} f})(\theta).$$

Now if f is C^∞ and of compact support,

$$h^{-2r} \Delta_h^{2r} f \to D^{2r} f \quad \text{as} \quad h \to 0$$

in L_1, where D^{2r} denotes the differentiation operator of order $2r$. Hence for each fixed θ we have that as $h \to 0$

$$2^{2r} h^{-2r} P_r(h\theta) \hat{f}(\theta) \to \theta^{2r} \hat{f}(\theta)$$

for all f in C^∞ of compact support. Consequently

$$P_r(\theta) = (\theta/2)^{2r}(1 + o(1)) \quad \text{as} \quad \theta \to 0$$

and, applying (50), (24) follows.

References

[1] R.L. Barakat and G.N. Newsam. Algorithms for reconstruction of partially known, bandlimited Fourier transform pairs from noisy data. I. The prototypical linear problem. *J. Integral Equ.* **9**, 49-76 ,1985.

[2] R.L. Barakat and G.N. Newsam. Algorithms for reconstruction of partially known, bandlimited Fourier transform pairs from noisy data. II. The nonlinear problem of phase retrieval. *J. Integral Equ.* **9**, 77-??,1985.

[3] M. Bertero, C. de Mol, and E.R. Pike (1985) Linear inverse problems with discrete data. I: General Formulation and Singular System Analysis. *Inverse Problems* **1** 301-330.

[4] M. Bertero and E.R. Pike (1982) Resolution in diffraction-limited imaging, a singular-value analysis. I: The case of coherent illumination. *Optica Acta* **29** 727-746.

[5] P.J. Bickel (1983) Minimax estimation of the mean of a normal distribution subject to doing well at a point. *Recent Advances in Statistics* 511-528. Academic Press.

[6] Donoho, D.L. (1988) One-sided inference about functionals of a density. *Annals of Statistics* **16**, 1390-1420.

[7] D.L. Donoho and I.M. Johnstone. Minimax Risk over l_p Balls. Technical Report 201, Department of Statistics, U.C. Berkeley. May 1989.

[8] D.L. Donoho, I.M. Johnstone, J.C. Hoch, and A.S. Stern. Does Maximum Entropy Improve Sensitivity? Technical Report, Department of Statistics, U.C. Berkeley, 1990.

[9] D.L. Donoho and P.B. Stark. Superresolution and Positivity Constraints: Computational Experiments. Technical Report, Department of Statistics, U.C. Berkeley, 1990.

[10] R. Freeman. *A Handbook of Nuclear Magnetic Resonance*, London: Longman Scientific Publishers, (1988).

[11] B.R. Frieden. Restoring with Maximum Entropy II. Superresolution of photographs with diffraction-blurred impulses. *Journal of the Optical Society of America* **62**, 1202-1210, (1972).

[12] B.R. Frieden. Dice, Entropy, and Likelihood. *Proc. IEEE* **73**, 1764-1770, (1985).

[13] S.F. Gull and G.J. Daniell. Image Reconstruction from incomplete and noisy data. *Nature* **272** 686-690, (1978).

[14] M. Harwit and N.J.A. Sloane. *Hadamard Transform Optics.* New York: Academic Press, (1979).

[15] J.C. Hoch, A.S. Stern, D.L. Donoho, and I.M. Johnstone. Reconstruction of complex, phase-sensitive spectra. To appear *Journal of Magnetic Resonance*, (1989).

[16] P.A. Jansson. *Deconvolution, with Applications in Spectroscopy.* Academic Press: New York, (1984).

[17] B.F. Logan (1965). *Properties of High-Pass Signals.* Ph. D. Thesis, Columbia University.

[18] R.H. Newman, Maximization of Entropy and Minimization of Area as Criteria for NMR signal Processing. *Journal of Magnetic Resonance* **79**, 448-460, 1988.

[19] E.R. Pike, J.G. McWhirter, M. Bertero, and C. de Mol. Generalized information theory for inverse problems in signal processing. *IEE Proceedings* **131** 660-667, 1984.

[20] M.S. Pinsker (1980) Optimal Filtration of square-integrable signals in Gaussian White Noise. *Problems of Information Transmission* 120-133.

[21] J.C. Sanz. Phase Recovery. *SIAM J. Appl. Math.* 1984.

[22] S. Sibisi, J. Skilling, R.G. Brereton, E.D. Laue, and J. Staunton. Maximum entropy signal processing in practical NMR spectroscopy. *Nature* **311**, 446-447, (1984).

[23] J. Redfearn, *The Times* (London), 16C, October 17,1984.

[24] J. Skilling and R.K. Bryan, *Mon. Not. R. Astr. Soc.* **211**, 111-124, (1984).

[25] J. Skilling, News and Views: The Maximum Entropy Method. *Nature* **309**, 748-749, (1984).

[26] D.M. Titterington, Letters to *Nature*: The maximum entropy method for data analysis. *Nature* **312**, 381-382, (1984) (and reply by J. Skilling)

[27] S.J. Wernecke and L.R. D'Addario. Maximum entropy image reconstruction. *IEEE Trans. Comput.* **C-26**, 351-364 (1977).

Table I: Maximum Risk over ϵ-Black Objects			
ϵ	$M(\epsilon)$	$M(l_1, \epsilon)$	$M(\delta_{exp}, \epsilon)$
.01	.046	.052	.20
.02	.078	.087	.27
.05	.153	.16	.42
.10	.248	.26	.56
.20	.390	.41	.72

Notes: Assumes $\sigma^2 = 1$. The raw data have worst case MSE $= 1$. $M(\delta_{exp}, \epsilon)$ denotes performance of Bayes rule for exponential prior with mean 3. (For comparison purposes).

Figure Captions

Figure 1.1 Reprinted from Figures 1-2, [22]. (a) Conventional FT-NMR reconstruction. (b) ME reconstruction for same data as (a). (c) FT-NMR reconstruction from a better experiment.

Figure 1.2 Reprinted from Figure 4, [11]. Best Linear Recovery from Noisy Data (—). Best Linear Recovery from Noiseless Data (....). ME Recovery from Noisy Data (solid). True object consists of two spikes at .33R spacing.

Figure 2.1 The nonlinearity $\delta_{ME,\lambda}$ for three different parameter values: $\lambda = \frac{1}{10}, \frac{1}{2}, 2$.

Figure 2.2 (a) Object x to be recovered. (b) Noisy data y from model (4); $\sigma = 1$, $n = 196$. (c) ME estimate $\hat{x}$ using $\lambda = \frac{1}{2}$.

Figure 2.3 Risk $\rho(\theta; \lambda, \sigma)$ with $\lambda = \frac{1}{2}$,$\sigma = 1$.

Figure 3.1 (a) FT NMR recovery of the real part of the spectrum of tryptophan. (b) Cambridge ME recovery of real part. (c) Recovery of real part resulting from applying a nonlinearity $\delta_{CME,\lambda}(y)$ elementwise to panel (a).

Figure 3.2 (a) Real part of the FT reconstruction from synthetic data. Data consist of two decaying sinusoids with line widths 1.0 and 1000.0 Hertz and amplitudes 100, 5000. Series length $n = 256$. (b) Real part of ME reconstruction for same data, using Cambridge method with $C_0 = 3.6 \times 10^7$.

Figure 4.1 Geometry of superresolution. The set of non-negative objects is a cone; the set of objects satisfying $||Kx' - Kx|| \leq \Delta$ is a cylinder. When the intersection of the cone and cylinder becomes small as $\Delta \to 0$, we say x admits superresolution.

Figure 1.1. Improvement of Signal to Noise Ratio

Panel a.

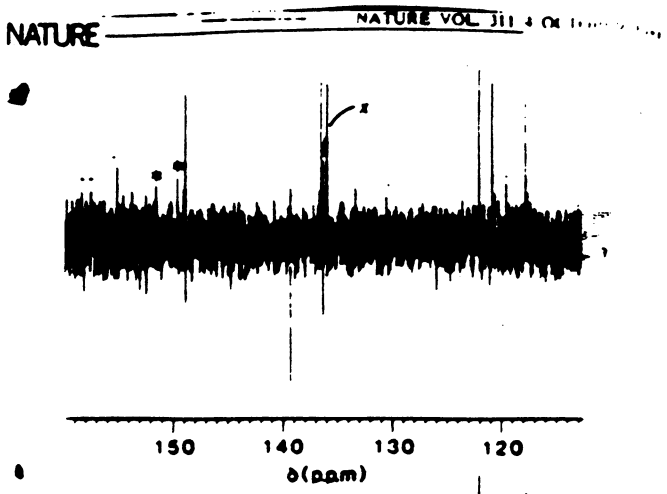

Panel b.

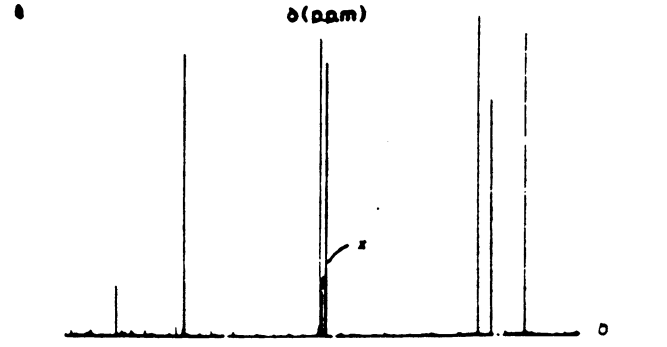

Fig. 1 *a*, Conventional Fourier transform of the ^{13}C FID produced by a pulse of 1.6 μs on a sample of 2-vinyl pyridine in $CDCl_3$. *b*, MEM spectrum from the same FID. ×, Instrumental artefact, attributed to imperfect transmitter gating

Panel c.

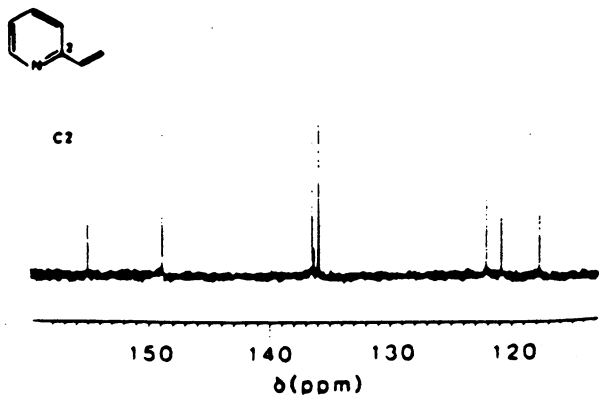

Fig. 2 Conventional Fourier transform of the ^{13}C FID produced by a pulse of 13 μs.

Figure 1.2. Super-Resolution

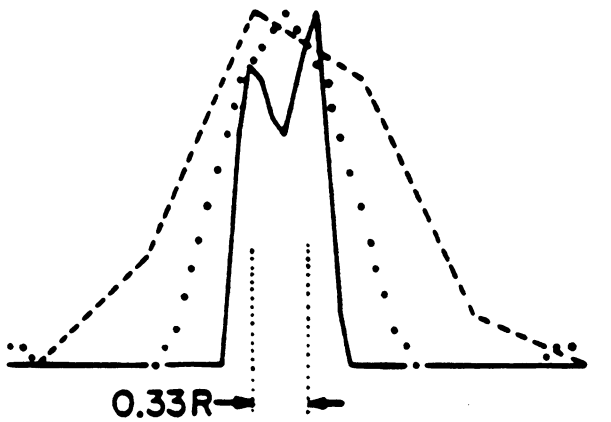

FIG. 4. Ideal image (- - -), its ME restoration (——), and perfect band-limited version (· · ·) for the two-slit object with $0.33R$ separation. Nonphysical negative portions of the (· · ·) curve are left out. Image (- - -) is not perfectly symmetric because it is not sampled symmetrically in y.

Figure 4.1

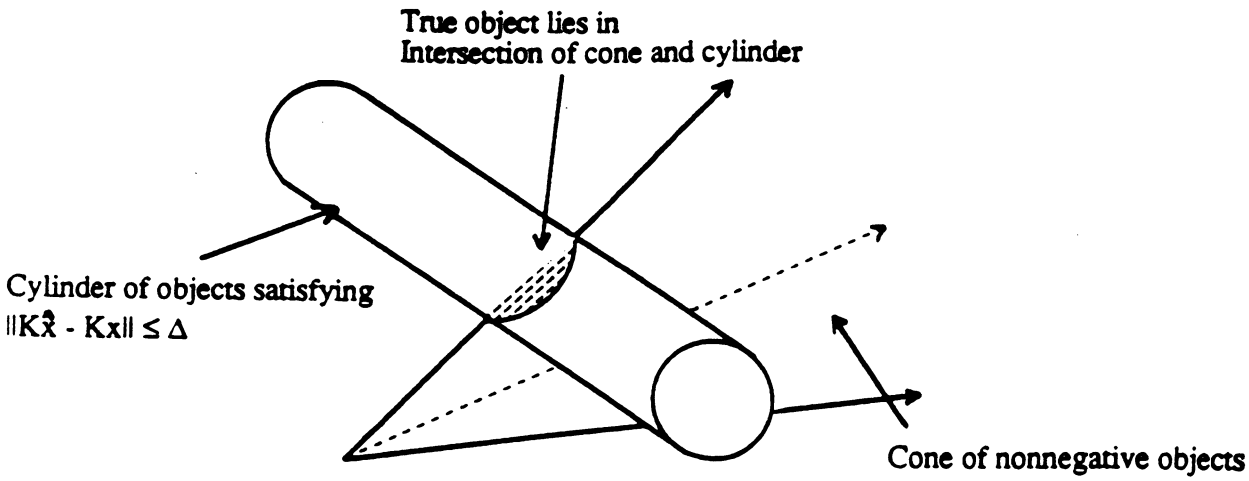
True object lies in
Intersection of cone and cylinder
Cylinder of objects satisfying
$\|K\hat{x} - Kx\| \leq \Delta$
Cone of nonnegative objects

Figure 3.2

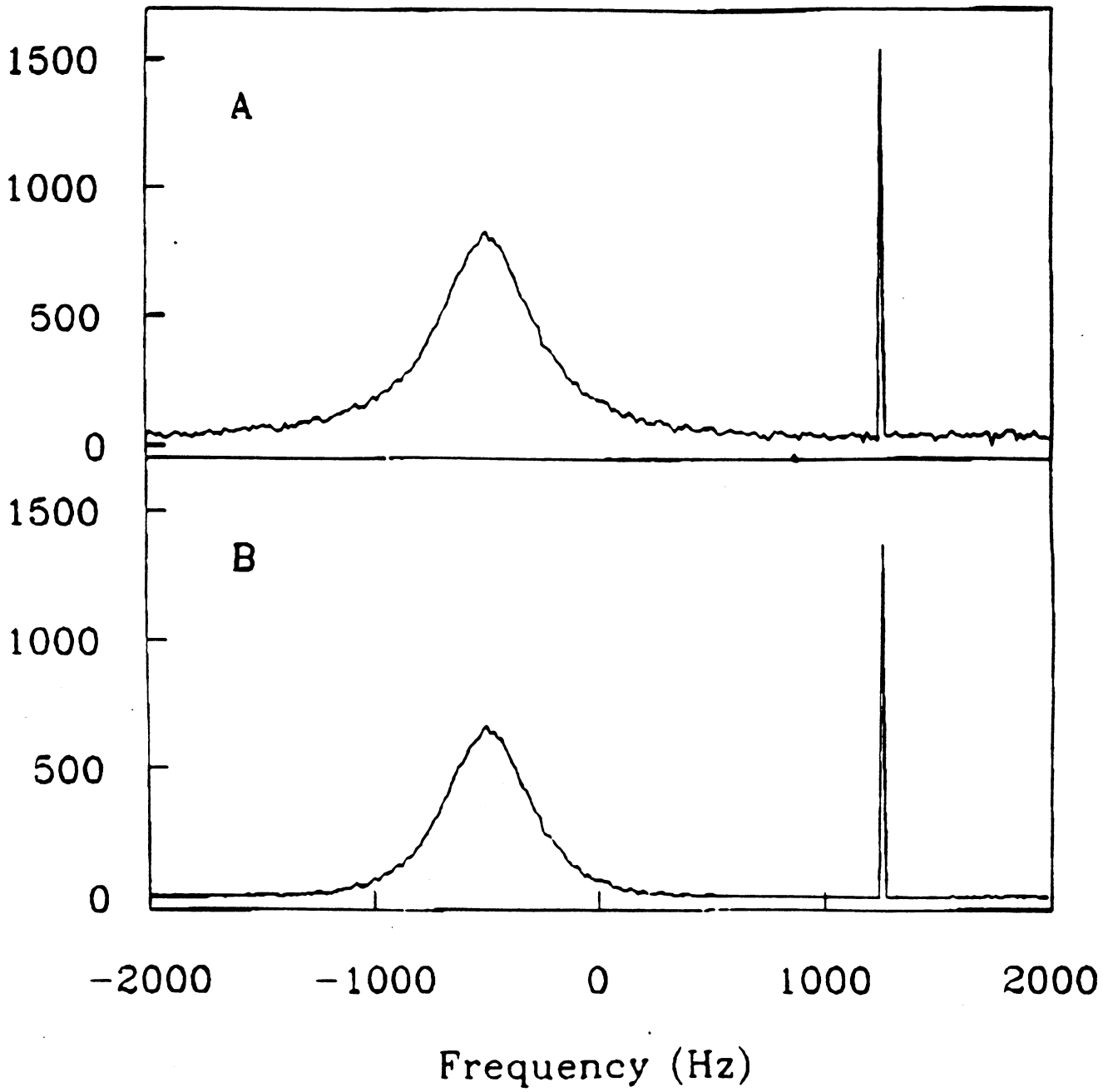
1500
A
1000
500
0
1500
B
1000
500
0
−2000
−1000
0
1000
2000
Frequency (Hz)

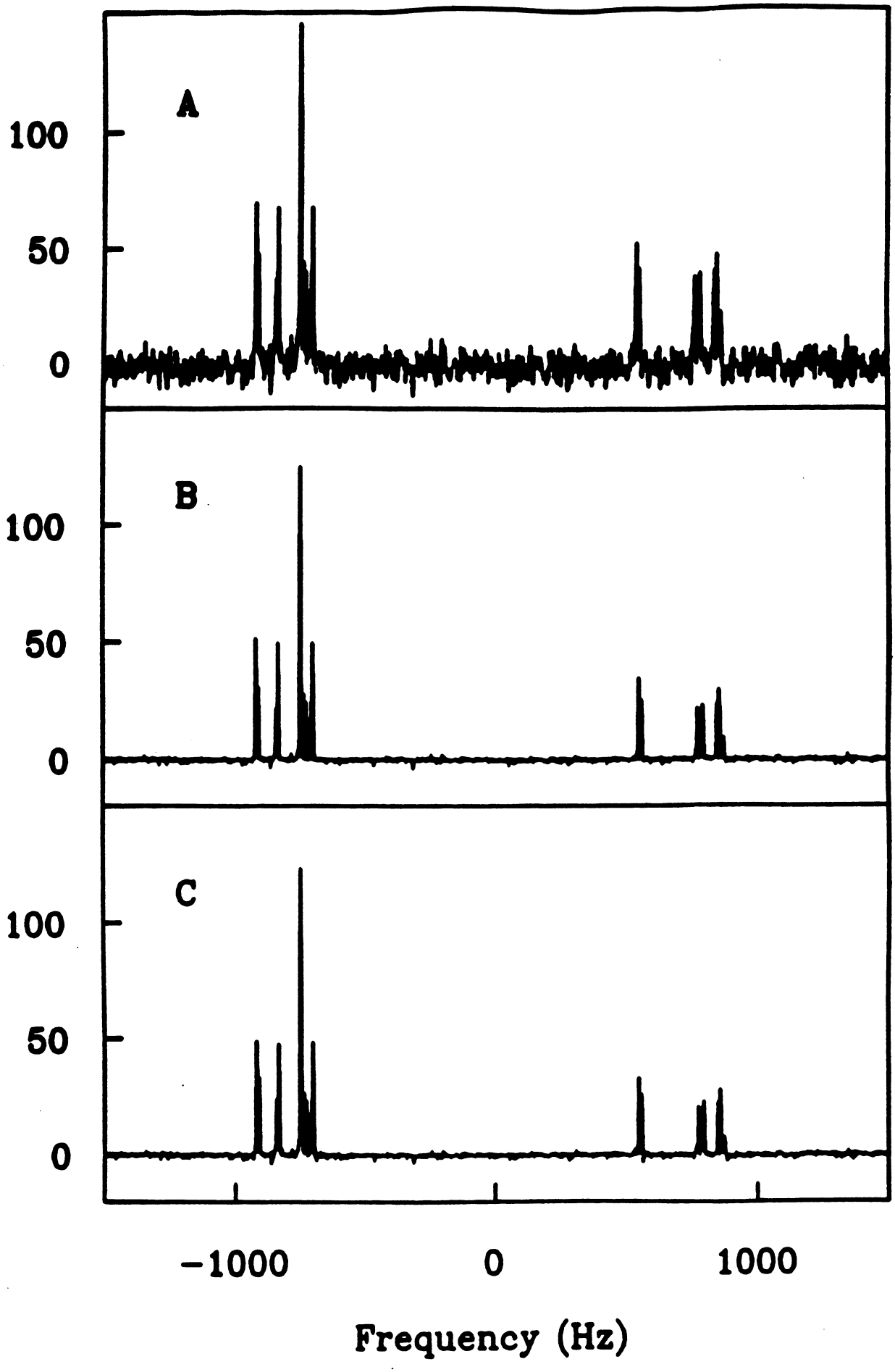
A
100
50
0
B
100
50
0
C
100
50
0
−1000
0
1000
Frequency (Hz)

Figure 2.3. Risk of ME rule

$\lambda = 1/2$, $\sigma = 1$

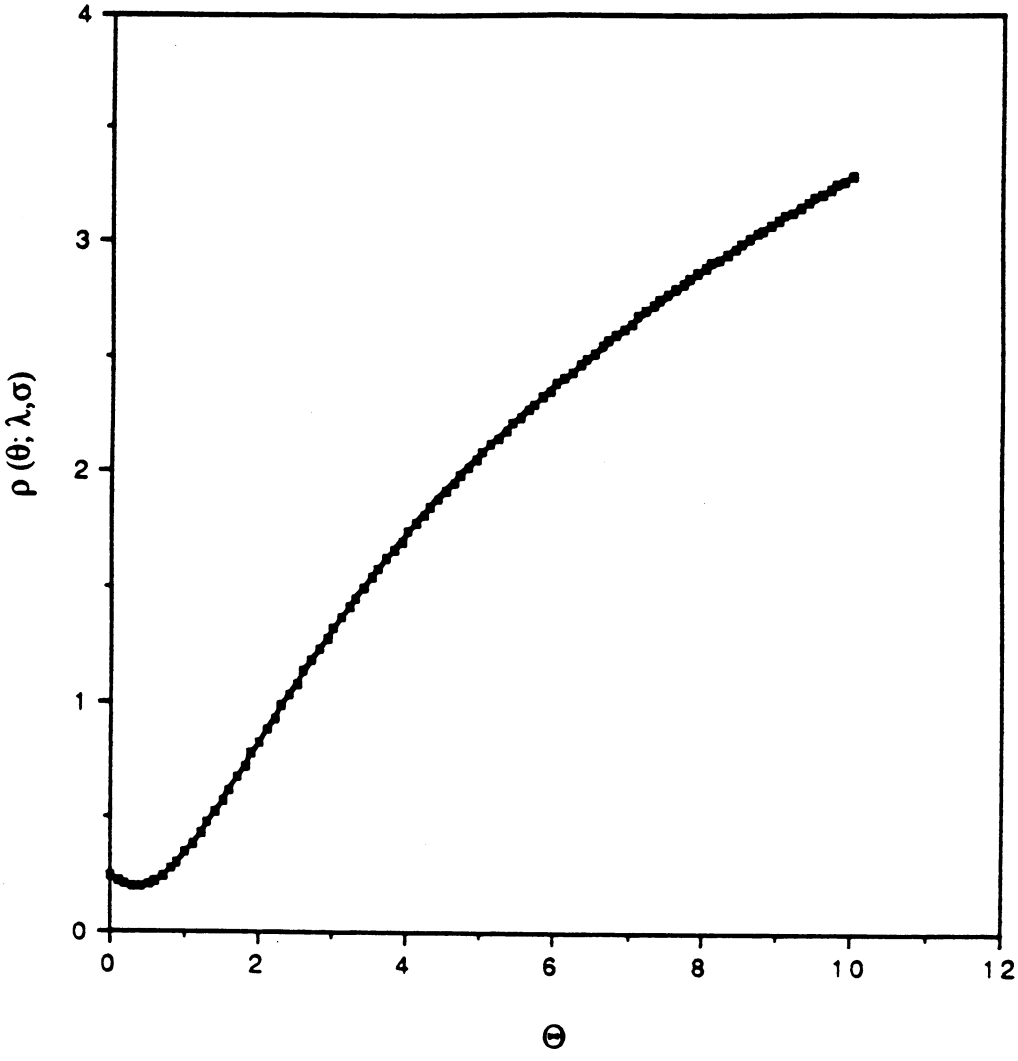

Figure 2.2: ME Recovery of Nearly-Black Object

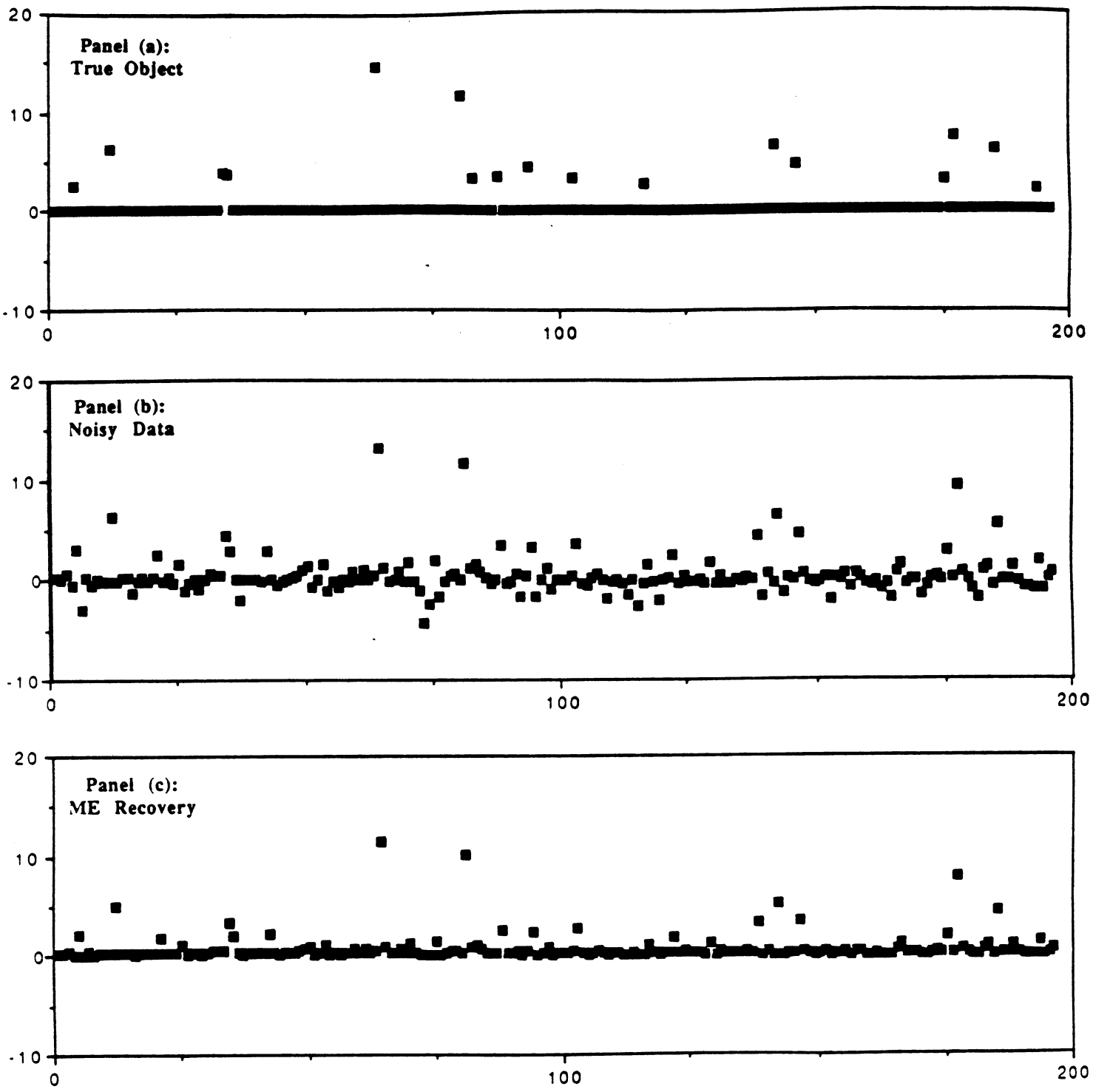

Figure 2.1. The ME Nonlinearity